Power Efficiency Enhancement in High-Boost Three-Phase Split Source Inverters

Safaa Ibrahim
Department of Electronics Technology, Faculty of Technology and Education, Beni-Suef University, Beni-Suef 62511, Egypt
safaaibrahim_pg@techedu.bsu.edu.eg

Samir A. Hamad
Department of Process Control Technology, Faculty of Technology and Education, Beni-Suef University, Beni-Suef 62511, Egypt
samireng46@techedu.bsu.edu.eg

Arafa S. Mansour
Electrical Engineering Department, Faculty of Engineering, Beni-Suef University, Beni-Suef 62511, Egypt
arafa.sayed@eng.bsu.edu.eg

Mohamed S. Zaky
Department of Electrical Engineering, College of Engineering, Northern Border University, Arar 1321, Saudi Arabia
mohamed.zaky@nbu.edu.sa (corresponding author)

Abdel-Gawad A. Abdel-Samei
Department of Electronics Technology, Faculty of Technology and Education, Beni-Suef University, Beni-Suef 62511, Egypt
dr_abdelgawad@techedu.bsu.edu.eg

Mostafa Wageh Lotfy
Department of Process Control Technology, Faculty of Technology and Education, Beni-Suef University, Beni-Suef 62511, Egypt
dr.mostafawag@techedu.bsu.edu.eg

Received: 21 February 2025 | Revised: 12 March 2025 | Accepted: 30 March 2025

 DOI: https://doi.org/10.48084/etasr.10670

ABSTRACT

This paper presents the design, analysis, and verification of a Split-Source Inverter (SSI) topology aimed at achieving efficient high-boost DC-AC power conversion with minimized power losses. The proposed design integrates an advanced control strategy utilizing Space Vector Modulation (SVM) to ensure clean sinusoidal output with minimal harmonic distortion. The study offers an in-depth examination of the SSI's operating principles, power loss mechanisms, and the distribution of losses across power switches, alongside optimization techniques to improve overall performance. Simulation results under diverse operating conditions validate the SSI's capability to deliver stable and efficient operation. Additionally, experimental implementation using a prototype validated the theoretical and simulation results, demonstrating the inverter's reliable operation and effective thermal management. Key findings underscore the significant advantages of the proposed SSI topology, including its compact design and superior performance compared to the quasi-Z-Source Inverter (q-ZSI). Specifically, the SSI reduces switching losses from 22% to 20% and decreases conduction losses from 42% to 38%, demonstrating enhanced efficiency, energy management, and applicability to diverse fields such as renewable energy systems and industrial drives.

Keywords-three-phase inverter; three-phase Split-Source Inverter (SSI); power loss; high gain

I. INTRODUCTION

Three-phase inverters are essential in various applications, including solar and wind energy systems, electrified vehicles, and industrial power systems. The most interesting topology among all inverter topologies is the Split-Source Inverter (SSI) because it can deliver the highest voltage conversion ratios with fewer components than those being used in a traditional transformer or multiple conversion stages. This method makes the SSI topology suitable for application areas where size, efficiency, and costs are critical factors [1]. Conventional inverter topologies, such as the Voltage Source Inverter (VSI) and the Current Source Inverter (CSI), face problems to amplify the low voltage DC to the needed level of AC voltage. The VSI for instance needs a big DC link capacitor for voltage buffering and in high boost applications, requires extra stages that cause additional complexity, size, and costs. The CSI, though designed to handle higher currents, is less efficient due to the losses associated with the inductive elements involved [2, 3].To address these challenges, the SSI topology was introduced, combining the benefits of both VSI and CSI in a simplified design with fewer passive components. Its unique split-source configuration enables single-stage DC-AC conversion with inherent voltage-boosting capability, making it particularly well-suited for low-voltage renewable energy applications. However, as demand grows for higher voltage gains in systems such as photovoltaic (PV) installations and Electric Vehicle (EV) chargers, advancements in SSI technology have become essential. This need for improved performance has driven the development of high-boost three-phase SSI, which enhances the standard SSI by delivering substantially higher voltage gains.

However, some potential knowledge gaps need to be overcome in order to take benefit of the high-boost SSI technology. Power losses control is one of the key issues, since it is especially relevant to the power switches. Because of high boost operation, power switches are exposed to higher voltages, increasing the on-state and switching current losses. These losses not only reduce the inverter efficiency but also lead to overheating of the components [6]. The second difficulty relates to the essential control strategy of the power electronic converter, which has to provide a stable operation at a very low input voltage. The growing complexity of the control algorithm required, in order to handle higher boosting and to effectively convert power, degrades the system losses and dynamic performance [7].

In the case of HB DC-AC conversion, some of the most effective solutions to overcome withering are listed below. Multi-stage inverters and cascaded H-bridge inverters have been used in order to increase the output voltage gain. These solutions have their drawback in the shape of extra size, cost and complexity or accomplishment. Cascaded H-bridge inverters, however, have relatively high voltage gain, but their efficiency is rather low because of the greater density of power switches and regulation circuits [8]. Other techniques have been attempted including the application of high frequency transformers or resonant converters to attain steep voltage multiplication. However, these methods cause extra losses and system complexity, especially in the transformer design and control or the resonant components. Also, high-frequency transformers have a tendency to produce high electromagnetic interference, which may not be easy to reduce especially when they are made small [9, 10]. In SSIs, the power switches experience higher voltage and current stresses due to the elevated boost ratios. This increases the conduction and switching losses, making it crucial to carefully select and design the power switches to minimize these losses. The loss distribution among the power switches is also of particular importance, as uneven loss distribution can lead to thermal hotspots, which can degrade the performance and reliability of the inverter [11].

This research paper presents a significant advancement in high-boost DC-AC power conversion through the development of a high-boost SSI featuring a simplified topology that eliminates the need for an external DC-DC converter [12]. This reduces overall system size and cost while maintaining high efficiency and robust performance. Unlike conventional designs, the high-boost -SSI employs a modified SVM control strategy to minimize converter losses and further enhance efficiency [13, 14]. The study provides a comprehensive power loss analysis and introduces advanced reduction strategies, including next-generation semiconductor materials, optimized control algorithms, and soft-switching techniques. Experimental validation using a prototype confirms the practicality of the proposed design, demonstrating its reliability and superior performance [15]. These findings underscore the high-boost SSI's potential for widespread application in renewable energy systems and industrial drives.

II. ANALYSIS OF SPLIT-SOURCE INVERTER TOPOLOGIES

Three-phase SSI has gained popularity in efficient DC-AC conversion, particularly in renewable energy systems, by connecting DC sources to boost voltage and improve output quality (Figure 1). While the SSI achieves superior voltage gain and reduced component count, the quasi-Z-Source Inverter (q-ZSI) remains a strong alternative with notable advantages. The q-ZSI enhances the conventional ZSI by adopting a modified impedance network that improves voltage gain, reduces voltage stress on switches, and maintains a continuous input current profile making it ideal for PV and fuel cell applications. Additionally, The VSI, although widely used in power conversion systems due to its simple control and minimal component count, requires an additional DC-DC boost stage to achieve high voltage gain, increasing system complexity and losses. However, despite these advantages, the q-ZSI typically requires more control tuning and achieves lower voltage gains than the SSI in high-boost applications. Table I compares the VSI, q-ZSI, and SSI, emphasizing their differences in component counts, shoot-through states, and DC voltage gain equations to highlight their design trade-offs and performance characteristics.

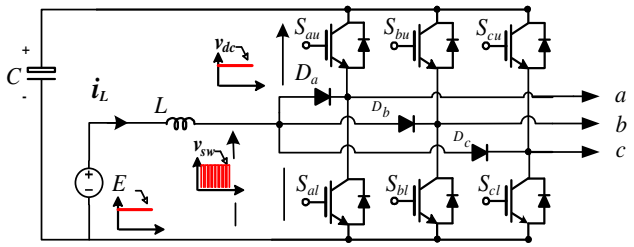

Fig. 1. The SSI.

TABLE I. COMPARISON OF TOPOLOGICAL DETAILS FOR ZSI, Q-ZSI, AND SSI STRUCTURES

Item description	VSI [13]	q-ZSI [19]	SSI
Number of stages	2	1	1
Number of input diodes	1	1	3
Number of input capacitors	1	2	1
Number of input inductors	1	2	1
Shoot-through states	Not Required	Required	Not required
Number of input switches	1	0	0
DC voltage gain	$\frac{1}{1-D}$	$\frac{1}{1-2D}$	$\frac{1}{1-D}$
Efficiency (%)	89%	93%	96%

A. *Modified SVPWMTechnique for SSI*

The modified SVM method effectively eliminates the low-frequency component present in both the inductor current and the inverter voltage. This is accomplished by maintaining a fixed duty cycle, calculated as the ratio of the active-state equivalent times T_a and T_b to the total switching time (T_s). The zero-state equivalent time (T_z) can be redistributed without altering the active-state times, as illustrated in the switching pattern of the SVPWM scheme shown in Figure 2. The process relies on reallocating T_z while preserving the active-state durations. Equation (1) defines the minimum zero-state equivalent time (T_{zm}), which corresponds to the inductor (L) discharge time T_x [2].

$$T_x = T_{zm} = T_s\{1 - 2M \sin(\pi/6)\} \quad (1)$$

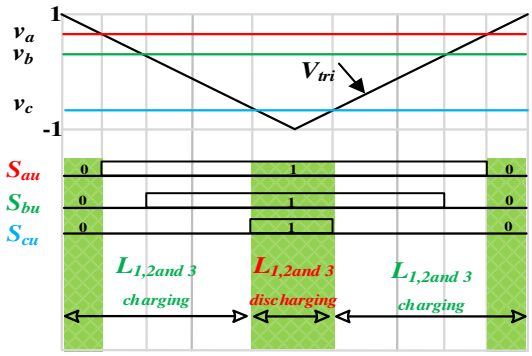

Fig. 2. Three-phase Space Vector Modulation (3Φ-SVM).

By setting T_x equal to T_{zm}, the same biasing approach discussed above is applied. This adjustment ensures that the reference signals remain constant at the lower virtual envelope, with the duty cycle D fixed at M. Based on this configuration, the normalized peak phase voltages of the inverter and the fundamental output can be determined through appropriate calculations [17].

B. *Power Loss Model of a Split-Source Inverter (SSI)*

The converter's primary power losses stem from its switching components, mainly due to the switching and conduction processes. At lower switching frequencies, conduction losses dominate, whereas switching losses become more significant at higher frequencies. In the case of an IGBT paired with a reverse diode, both components experience conduction losses, attributed to their on-state resistance and reverse voltage. While these parameters may exhibit slight variations with temperature, they are typically considered constant for simplification in analysis. The reverse voltages of the transistor and diode are denoted as V_{RT} , and V_{RD} , respectively, while their internal resistances are represented as R_{IT} and R_{ID}.The average conduction losses of the transistor and diode, denoted by $P_{CL}{}^{T}$, and $P_{CL}{}^{D}$, can be expressed as [18]:

$$P_{CL}{}^{T} = \frac{1}{T}\int_0^T \left(V_{RT} + R_{IT} \cdot i^{\beta}(t)\right) \cdot i(t) \cdot dt$$
$$P_{CL}{}^{D} = \frac{1}{T}\int_0^T \left(V_{RD} + R_{ID} \cdot i^{\beta}(t)\right) \cdot i(t) \cdot dt \quad (2)$$

where T represents the fundamental cycle, β is the constant associated with the transistor, and $i(t)$ refers to the current passing through the transistor or the diode. The total conduction losses are expressed as:

$$P_{C_{\text{tot}}} = P_{CL}{}^{T} + P_{\text{CL}}{}^{D} \quad (3)$$

Switching losses represent the power dissipated by each switch and diode during their ON and OFF states. The energy loss for a single switch can be formulated as:

$$E_{ON} = \frac{1}{T}\int_0^{t_n} v(t) \cdot i(t) \cdot dt = \frac{1}{6} \cdot V_s \cdot I \cdot t_n$$
$$E_{OFF} = \frac{1}{T}\int_0^{t_f} v(t) \cdot i(t) \cdot dt = \frac{1}{6} \cdot V_s \cdot I \cdot t_f \quad (4)$$

where E_{ON} and E_{OFF} represent the energy dissipated during the turn-on and turn-off periods, respectively, while t_n and t_f correspond to the durations of the ON and OFF states. V_s denotes the voltage across the switch before or after the transition periods. The total switching losses can be expressed as:

$$P_{SW}{}^{T} = \sum_{\text{n}^{th}}^{N_{MO}} (E_{ON} + E_{OFF}) \quad (5)$$

where N_{MO} is the total number of IGBTs in the inverter, and n^{th} refers to the switch number. Switching losses in diodes are neglected, as they are considered to operate with soft-switching [16]. The average total losses of the inverter are given by:

$$P_{\text{L-tot}} = P_{\text{Ctot}} + P_{\text{Sw}}{}^{T} \quad (6)$$

III. RESULTS AND DISCUSSION

A. *Simulation Results*

To perform a more detailed analysis of the topology, MATLAB-SIMULINK® was utilized, applying the parameters outlined in Table II to enable a comprehensive evaluation. The studied topologies of the three-phase inverters were designed to

supply power to a three-phase inductive load, characterized by a 10 Ω resistor connected in series with a 5 mH inductor. The system was powered by a low-voltage DC source, with an input voltage of 100 V, which could represent a PV panel under simulation conditions. To ensure precise switching control, a leading-edge saw tooth carrier waveform with a frequency of 10 kHz was employed. For the SSI configuration, the DC-link circuit was designed with an inductance of 3-mH and a capacitance of 470 µF, optimizing the system for effective energy conversion and stability. The simulation results, presented in Figure 3, provide a comprehensive analysis of the inverter's performance. These results include waveforms for inverter phase and line voltages, output line currents, inductor current, capacitor voltage, and DC-link voltage. The simulation also evaluates the power loss distribution across the topology, offering valuable insights into the efficiency and operational dynamics of the SSI.

TABLE II. ELEMENTS USED TO SIMULATE THE ANALYZED TOPOLOGY

Element	SSI
M	0.6
F_I	10000 Hz
F_O	50 Hz
Capacitances and inductance	$C_1, C_2 = 470$ µF $L_1 = 3$ mH
DC voltage	100 V

TABLE III. POWER LOSS DISTRIBUTION COMPARISON

Quantity	q-ZSI [13]	SSI
Switching losses $P_{SW}{}^{T} = \sum_{n^m}^{N_{MO}} (E_{ON} + E_{OFF})$	22%	20%
Conduction losses $P_{C_{tot}} = P_{CL}{}^{T} + P_{\mathrm{CL}}{}^{D}$	42%	38%

The switching and conduction losses of the single-stage SSI have been thoroughly evaluated. Figure 3(f) illustrates the total loss variation with respect to load power using a leading-edge sawtooth carrier, with input voltage set to $v_{in} = 100$ V. Additionally, Figure 3(f) illustrates the distribution of power losses across various switches at full load, revealing that the input diodes account for nearly half the total losses. Replacing these diodes with MOSFETs, as suggested in [19, 20], could greatly enhance the system efficiency. The variation in total losses relative to load power for the SSI is also shown in Figure 3(f), along with Table III, which compares the power loss distribution between the q-ZSI and SSI. Notably, if the shoot-through state occurs only once per cycle, the required inductance would increase significantly. Moreover, the q-ZSI diode experiences higher losses due to the increased current stress it must withstand.

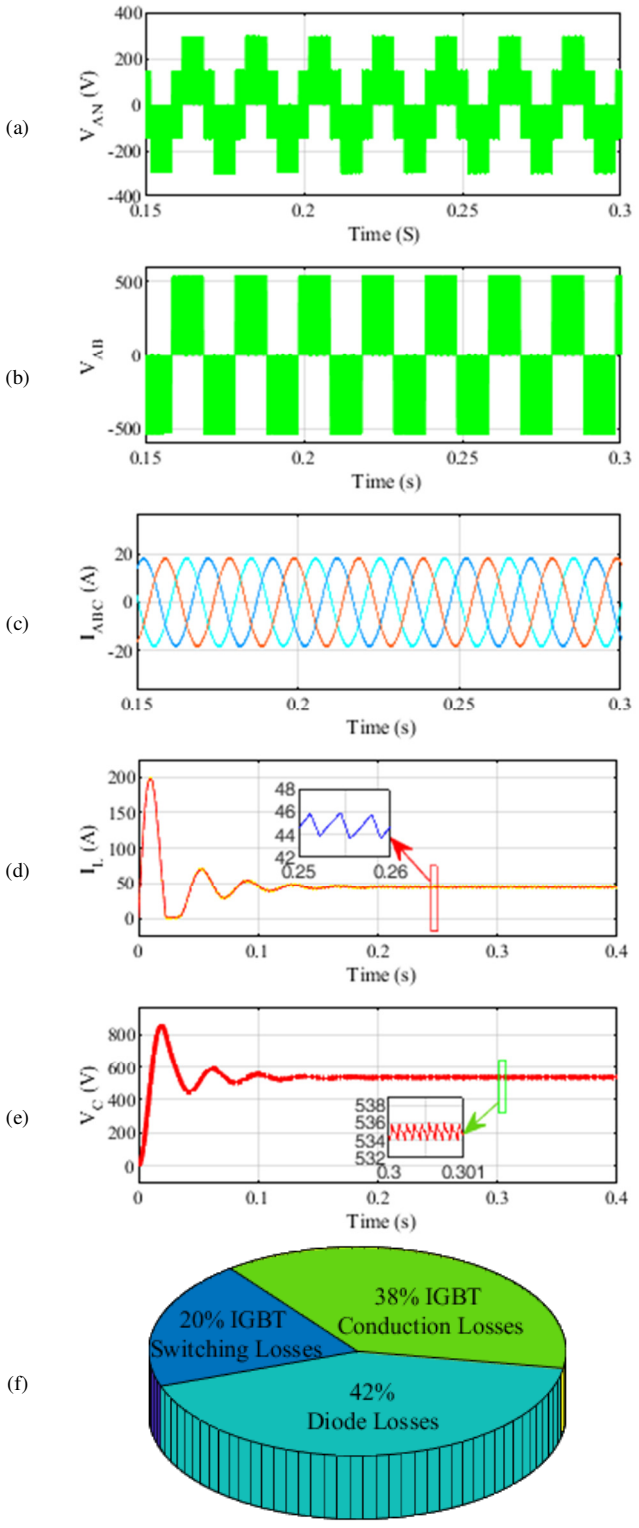

Fig. 3. Simulation results of the SSI using the proposed SVM strategy: (a) Inverter phase voltage, (b) output line voltage, (c) inverter line currents, (d) inductor current, (e) capacitor voltage waveforms, and (f) power loss distribution of the SSI.

B. Experimental Validation

To validate the performance of the analyzed topology, a prototype of the SSI was designed and implemented. The parameters used in the prototype are outlined in Table IV, while the experimental setup is illustrated in Figure 4. The SSI prototype was built using the Texas Instruments LaunchPad LAUNCHXL-F28379D DSP board, which facilitated the generation of gating pulses for modified SVM and incorporated a dead-time setting of 1.5 µs. For this implementation, the inductor and capacitor values were chosen as 2.5 mH and 150 µF, respectively. This experimental configuration provides a robust platform for in-depth testing and analysis of the SSI's performance. It enables a detailed examination of its operational characteristics, such as efficiency, output waveform quality, and dynamic response. Furthermore, the insights gained from this setup highlight the potential of the SSI for practical applications in advanced power conversion systems.

TABLE IV. EXPERIMENTAL PARAMETERS FOR THE SSI

Parameter	Value	Parameter	Value
Switching frequency	10 kHz	DSP	TI-F28379D
Dead time	1.5 µs	*M*	0.6
Inductor	2.5 mH	Load	10 Ω and 5 mH
Capacitor	150 µF/400 V		

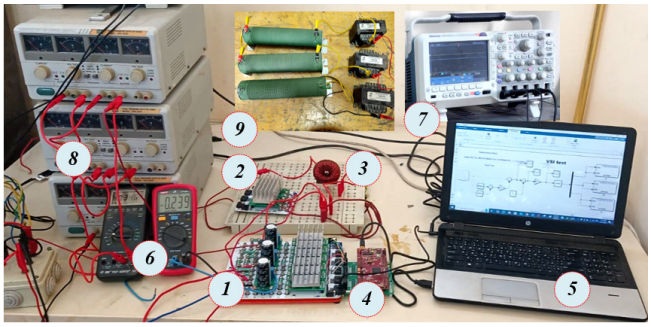

Fig. 4. Photographs of the experimental setup: (1) six IGBTs module, (2) three diodes module, (3) inductor, (4) F28379D Launchpad Kit Card™, (5) laptop, (6) digital multimeter, (7) oscilloscope ,(8) DC supply, and (9) RL-loads.

Figure 5 shows the experimental results obtained from the three-phase SSI operating under the proposed modified SVM strategy. The comprehensive analysis of the waveforms and measurements provides valuable insights into the performance of the system. Figure 5(a) displays the steady-state DC input current alongside the output line currents (I_a, I_b, I_c). The sinusoidal nature of the output line currents highlights the effectiveness of the modified SVM strategy in ensuring high-quality AC output with minimal distortion.

(a)

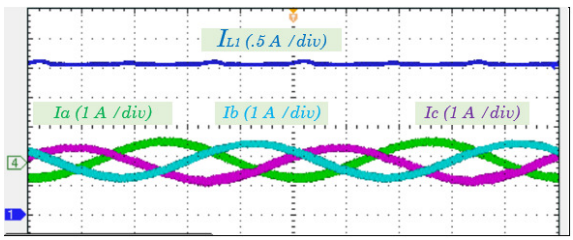

(b)

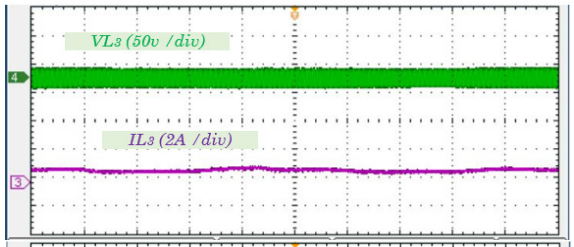

(c)

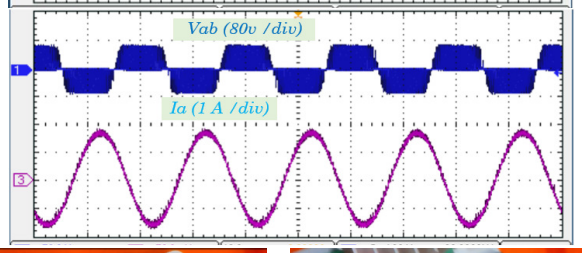

(d)

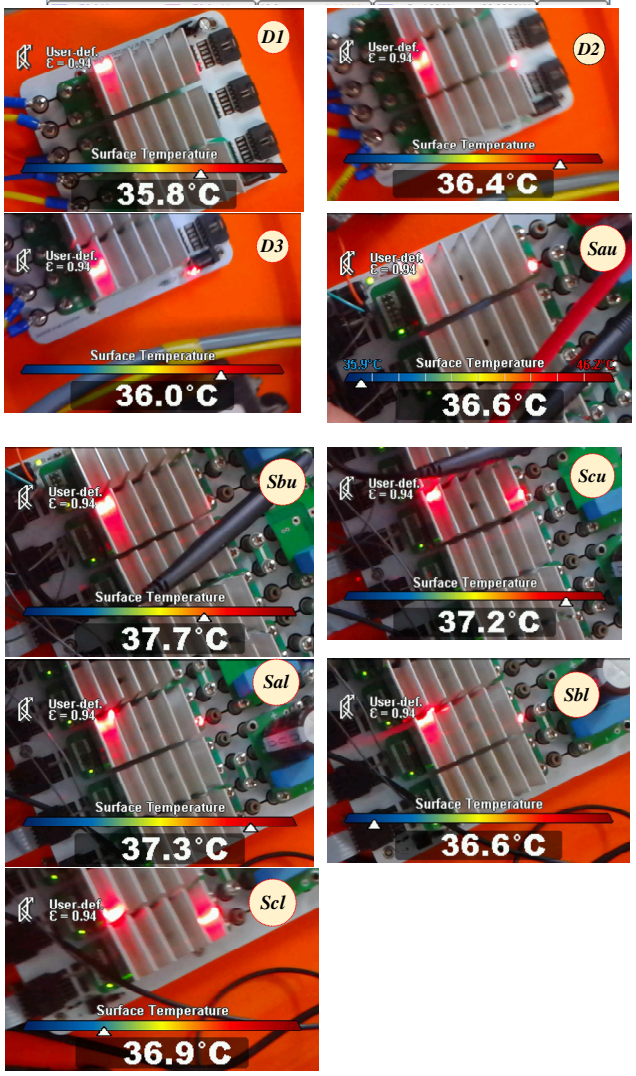

Fig. 5. Obtained experimental results of the three-phase SSI using the proposed SVM strategy, where (a) DC current and output line currents, (b) voltage and current across the input inductor, (c) line voltage and output line current I_a waveforms, and (d) temperature measured on six IGBT modules and three diodes modules.

The balanced amplitudes and phase alignment of the currents further validate the reliability of the inverter in handling three-phase loads. Figure 5(b) shows the voltage and current waveforms across the input inductor, providing insights into the energy transfer process within the inverter. The results reveal smooth transitions and stable operation, indicating that the design of the input inductor effectively manages the ripple and maintains energy balance. In Figure 5(c), the line voltage and the corresponding output line current (I_a) are depicted, demonstrating a strong correlation between the generated voltage and current. The sinusoidal nature of the waveforms, with negligible harmonics, highlights the efficiency of the modulation strategy in producing clean output power suitable for sensitive applications. Figure 5(d) presents the temperature measurements of the six IGBTs module and the three diodes module during operation. The results show that the thermal management system maintains module temperatures within safe operating limits, ensuring system reliability and longevity. The observed temperature uniformity among the modules indicates balanced power distribution and effective cooling mechanisms. The experimental results confirm the robust performance of the proposed SVM strategy in driving the three-phase SSI.

IV. CONCLUSIONS

This paper investigates the design, implementation, and performance assessment of a three-phase Split-Source Inverter (SSI) utilizing a proposed modified Space Vector Modulation (SVM) strategy. Through a detailed study involving theoretical analysis, simulation, and experimental validation, the research emphasizes the notable benefits and practical applications of the SSI topology. Experimental findings demonstrate that the SSI, when integrated with the modified SVM strategy, achieves high-quality sinusoidal output currents and voltages with minimal distortion. Furthermore, the SSI shows improved efficiency compared to the quasi-Z-Source Inverter (q-ZSI), reducing switching losses from 22% to 20% and conduction losses from 42% to 38%. The balanced operation and precise control of output waveforms validate the inverter effectiveness in managing three-phase loads. Additionally, the stable behavior of the input inductor and DC link underscores the system' robustness in maintaining energy balance and ripple control.

ACKNOWLEDGEMENT

The authors extend their appreciation to the Deanship of Scientific Research at Northern Border University, Arar, KSA for funding this research work through the project number NBU-FFR-2025-1250-02.

REFERENCES

[1] R. Haghi, R. Beiranvand, and M. Shahbazi, "A Quasi-Z-Source Four-Switch Three-Phase Inverter With Null Vector Capability," *IEEE Transactions on Industrial Electronics*, vol. 70, no. 6, pp. 5421–5432, Jun. 2023, https://doi.org/10.1109/TIE.2022.3198238.

[2] A. Chaaira, H. Kraiem, R. Gamoudi, and L. Sbita, "Comparative Analysis of Bipolar and Unipolar SPWM Techniques in PIC-Based Pure Sine Wave Single-Phase Inverters," *Engineering, Technology & Applied Science Research*, vol. 14, no. 3, pp. 14395–14401, Jun. 2024, https://doi.org/10.48084/etasr.7150.

[3] A. Radhika, K. V. Kumar, and A. Prakash, "Hybrid control for capacitor-assisted Z-source inverter in grid-connected photovoltaic system," *Renewable and Sustainable Energy Reviews*, vol. 208, Feb. 2025, Art. no. 115002, https://doi.org/10.1016/j.rser.2024.115002.

[4] G. Boztas, M. Yildirim, and O. Aydogmus, "Design and Analysis of Multi-Phase BLDC Motors for Electric Vehicles," *Engineering, Technology & Applied Science Research*, vol. 8, no. 2, pp. 2646–2650, Apr. 2018, https://doi.org/10.48084/etasr.1781.

[5] Q. T. An, L. Sun, K. Zhao, and T. M. Jahns, "Scalar PWM algorithms for four-switch three-phase inverters," *Electronics Letters*, vol. 46, no. 13, pp. 900–902, Jun. 2010, https://doi.org/10.1049/el.2010.0612.

[6] A. Abdelhakim, P. Mattavelli, and G. Spiazzi, "Three-Phase Split-Source Inverter (SSI): Analysis and Modulation," *IEEE Transactions on Power Electronics*, vol. 31, no. 11, pp. 7451–7461, Aug. 2016, https://doi.org/10.1109/TPEL.2015.2513204.

[7] D. Sun, Z. He, Y. He, and Y. Guan, "Four-Switch Inverter Fed PMSM DTC with SVM approach for Fault Tolerant operation," in *2007 IEEE International Electric Machines & Drives Conference*, Antalya, Turkey, Feb. 2007, pp. 295–299, https://doi.org/10.1109/IEMDC.2007.382682.

[8] Y.-C. Liu, X.-L. Ge, J. Zhang, and X.-Y. Feng, "General SVPWM strategy for three different four-switch three-phase inverters," *Electronics Letters*, vol. 51, no. 4, pp. 357–359, 2015, https://doi.org/10.1049/el.2014.4397.

[9] S. A. Hamad, W. Xu, M. W. Lotfy, A. K. Junejo, and M. A. Ghalib, "An improved model predictive control for linear induction machine drive-based split-source inverters," *Discover Applied Sciences*, vol. 6, no. 5, p. 220, Apr. 2024, https://doi.org/10.1007/s42452-024-05872-8.

[10] C. Xu and S. Lu, "Practical online modulation method for current ripple and switching losses reduction in the three-phase voltage source inverters", *IEEE Transactions on Power Electronics*, vol. 36, no. 2, pp. 1475-1490, 2021, https://doi.org/10.1109/TPEL.2020.3009824.

[11] B. Hajoary and R. Das, "Review on topologies of quasi Z-source inverter in grid-connected solar photovoltaic system," *Environment, Development and Sustainability*, Jan. 2025, https://doi.org/10.1007/s10668-025-05978-y.

[12] A. Hintz, U. R. Prasanna and K. Rajashekara, "Comparative study of the three-phase grid-connected inverter sharing unbalanced three-phase and/or single-phase systems", *IEEE Transactions on Industry Applications*, vol. 52, no. 6, pp. 5156-5164, 2016, https://doi.org/10.1109/TIA.2016.2593680.

[13] G. M. Cocco, F. B. Grigoletto, L. G. Scherer *et al.*, "Modeling and control of hydro-PV hybrid power system with three-phase three-leg split-source inverter", *Journal of Control, Automation and Electrical Systems*, vol. 33, pp. 1563–1575, 2022, https://doi.org/10.1007/s40313-022-00911-4.

[14] M. Hammami, R. Mandrioli, A. Viatkin, M. Ricco and G. Grandi, "Analysis of input voltage switching ripple in three-phase four-wire split capacitor PWM inverters", *Energies*, vol. 13, no. 19, 2020, Art. no. 5076, https://doi.org/10.3390/en13195076.

[15] S. Paul and K. Basu, "A three-phase inverter based overmodulation strategy of asymmetrical six-phase induction machine", *IEEE Transactions on Power Electronics*, vol. 36, no. 5, pp. 5802-5817, 2021, https://doi.org/10.1109/TPEL.2020.3026816.

[16] M. W. Lotfy, S. M. Dabour, R. M. Mostafa, D. J. Almakhles and M. F. Elmorshedy, "Modeling and control of a voltage-lift cell split-source inverter with MPPT for photovoltaic systems", *IEEE Access*, vol. 11, pp. 54699-54712, 2023, https://doi.org/10.1109/ACCESS.2023.3280602.

[17] Y. Jiang, J. Zhang, Q. Wang, F. He, and W. Zhang, "A Common-Mode Voltage Reduction PWM Strategy for Three-Phase Quasi-Z-Source Inverter With Optimized Switching Losses," *IEEE Access*, vol. 11, pp. 91891–91903, 2023, https://doi.org/10.1109/ACCESS.2023.3308148.

[18] C. Xu and S. Lu, "Practical Online Modulation Method for Current Ripple and Switching Losses Reduction in the Three-Phase Voltage Source Inverters," *IEEE Transactions on Power Electronics*, vol. 36, no. 2, pp. 1475–1490, Oct. 2021, https://doi.org/10.1109/TPEL.2020.3009824.

[19] M. Zarrinehbafan, A. Seifi, A. Nadermohammadi, and S. H. Hosseini, "A new single magnetic core coupled-inductor based active switched

Quasi Z-source inverter," *Scientific Reports*, vol. 14, no. 1, Jul. 2024, Art. no. 17197, https://doi.org/10.1038/s41598-024-68194-0.

[20] A. Abramovitz, B. Zhao, and K. M. Smedley, "High-Gain Single-Stage Boosting Inverter for Photovoltaic Applications," *IEEE Transactions on Power Electronics*, vol. 31, no. 5, pp. 3550–3558, Feb. 2016, https://doi.org/10.1109/TPEL.2015.2457454.